Noname manuscript No.
(will be inserted by the editor)

The impact of footprints of large-scale outer structures on the near-wall layer in the presence of drag-reducing spanwise wall motion

Lionel Agostini · Michael Leschziner

Received: date / Accepted: date

Abstract This study is motivated by the observation that the drag-reduction effectiveness achieved by the imposition of oscillatory spanwise wall motion declines with Reynolds number. The question thus posed is whether the decline is linked to the increasingly strong influence of large-scale outer structures in the log layer on the near-wall turbulence, in general, and the streak strength in the viscosity-affected layer, in particular – a process referred to as *modulation*. This question is addressed via an extensive statistical analysis of DNS data for a channel flow at a friction Reynolds number 1020, subjected to oscillatory spanwise wall motion at a nominal wall-scaled period of 100. The analysis rests on a separation of turbulent scales by means of the *Empirical Mode Decomposition*. This method is used to derive conditional statistics of small-scale motions and skin friction subject to prescribed intensity of large-scale motions – referred to as *footprinting*. It is shown that the large-scale fluctuations are responsible, directly on their own, for roughly 30% to the skin friction. Positive large-scale fluctuations are also shown to be the cause of a major amplification of small-scale streaks, relative to weak attenuation by negative fluctuations. This highly asymmetric process is likely to be indirectly influential on the drag-reduction process, although it is not possible to identify this indirect effect in quantitative terms as part of the present analysis.

Keywords Friction-drag reduction. Spanwise oscillatory wall motion. Large-scale outer structures. Small-scale modulation.

Lionel Agostini
Department of Aeronautics
Imperial College London
South Kensington, London, SW7 2AZ, UK
E-mail: l.agostini@imperial.ac.uk

Michael Leschziner
Department of Aeronautics
Imperial College London
South Kensington, London, SW7 2AZ, UK
E-mail: mike.leschziner@imperial.ac.uk

1 Introduction

A substantial number of DNS studies, the large majority for channel flow (e.g. [32,33,41,39,7,6,13,10] provide unambiguous evidence that various combinations of oscillatory and spatially-periodic spanwise wall motions, constituting streamwise travelling waves, give rise to substantial reductions in streamwise skin friction. Within this subject area, the so-called "Quadrio map" [33], charting the dependence of the drag-reduction margin on the oscillation frequency and the streamwise wave length of the spanwise motion, has attained a near-iconic status in the literature on skin-friction control. This map, derived from a large number of DNS computations for the rather low friction Reynolds number, $Re_\tau = 200$, shows that the skin friction can be reduced by up to 45%, subject to optimum actuation parameters (wall-scaled actuation period and streamwise wave length). Somewhat lower margins have been recorded in spatially developing boundary layers ([34,36,43,37,22,38]), but these have only been investigated with purely oscillatory wall motion.

An issue that has received much less attention is the Reynolds-number dependence of the drag-reduction margin. In large part, this is due to the rapid rise in the computational costs DNS demands as the Reynolds number increases. As a consequence, there have been very few simulations for $Re_\tau > 1000$, especially such performed over credibly large domains, in which case streamwise and spanwise periodicity can be regarded as realistic and credible from an accuracy point of view. This challenge becomes substantially more severe due to the need to accommodate large streamwise wave length and/or a sufficiently large oscillation periods, the latter especially pertinent when reliable phase-averaged statistics are to be extracted from the data ([7,6]. The highest Reynolds number reported so far is $Re_\tau = 2100$ (Gatti and Quadrio [13], but this simulation was performed over a very small domain of dimensions $1.2h \times 2h \times 0.6h$. Much bigger domains were used in simulations by Hurst et al [18] for the range $Re_\tau = 200 - 1600$.

Although studies reporting simulations at elevated Reynolds numbers (say, higher than $Re_\tau = 500$) adopted a variety of actuation scenarios, in terms of time-dependence, frequency and wave length, the overall picture emerging is that the drag-reduction margin tends to decline with increasing Reynolds number at a rate $Re_\tau^{-\alpha}$, where α depends greatly on the actuation parameters and the details of the simulation, but is in the range 0.15-0.3. An observation made by Hurst et al [18] and Gatti and Quadrio [14] is that the upward shift ΔU^+ in the velocity log-law, always observed with drag-reducing wall actuation when plotted with the actual, actuation-modified, wall shear stress, tends to become constant beyond $Re_\tau \approx 1000$, confirming a suggestion made by Luchini [26] on the basis of a simple analysis that links the thickness of the viscous sublayer to a given drag-reduction level. This result may be claimed to suggest that the physical processes in the viscous sublayer underpinning drag-reduction are not adversely affected by any distortions that arise from outer structures interfering with the turbulent state close to the wall.

Although the above inference pertains, importantly, to the drag reduction, rather than to the drag itself, its validity, if proven, would be astonishing in the light of many recent observations on the effects of outer-layer turbulence on the near-wall region arising from studies on canonical (unforced) boundary layers and channel flows, pursued entirely independently from drag-reduction scenarios. Such studies, both experimental and computational in nature, demonstrate, without ambiguity, that outer structures in the log-law region, the energy of which rises steady with increasing Reynolds number, impact strongly on the turbulence properties of the near-wall layer. The outer structures of highest visibility and thus greatest interest are quasi-organized "super streaks" with streamwise length scale of order $10h$ and spanwise separation of order $1h$. Mathis et al [28] proposed, on the basis of hot-wire measurements over a wide range of Reynolds numbers, that these energetic structures are located at $y^+ = 3.9\sqrt{Re_\tau}$, thus typically at $0.1-02h$. Extensive experimental work by Marusic, Mathis, Hutchins and their collaborators [20,29,27,19] has demonstrated, mostly with the aid of hot-wire techniques, that the outer structures affect the near-wall turbulent fluctuations in two ways: by "footprinting" and "modulation". The former is a process by which the outer large-scale motions impart correspondingly large translational fluctuations close to the wall, with some streamwise lag between the two — in essence, resulting in a near-wall field that is a superposition of large-scale footprints and the locally generated small-scale motions. The footprinting process is brought out clearly in figure 1, which arises from the a simulation for actuated channel flow at $Re_\tau = 1020$, discussed extensively later in detail. The images show streamwise-velocity fluctuations across three wall-parallel planes, at different wall-normal **positions.** The essential feature to note in the figure is the correspondence across the near-wall layer of spatially correlated large areas of predominantly elevated and depressed streamwise-velocity fluctuations, separated by roughly $\Delta z^+ \approx 1000$ and subject to a streamwise lag of roughly $\Delta x^+ \approx 500$. Modulation is a more subtle phenomenon, wherein the large-scale motions amplify or attenuate the small-scale turbulence depending on the sign of the large-scale footprints. Figure 1(a) also provides clear qualitative indications of modulation, in so far as the regions of high-velocity large-scale footprints features well-established small-scale streaks – **here inclined due to the spanwise Stokes strain induced by a streamwise-homogeneous, oscillatory spanwise wall motion,** $W(t) = W_m \sin(2\pi t/T)$ – while the low-velocity large-scale footprints lack distinct streaky structures or contain very weak streaks.

The statistical characterization of the correlation between the large-scale motion and the modulation is the subject of several recent experimental and computational studies, among them [29,27,35,18,8,5,44]. All deal, in one way or another, with the correlation between the outer large-scale motions and the turbulent state in the inner layer. Analysing DNS data for canonical channel flow at $Re_\tau = 1000 - 4200$, Agostini and Leschziner [5,3,2] demonstrate, in particular, that the modulation of small-scale near-wall turbulence by outer motions is highly asymmetric, with the amplification induced by footprints of

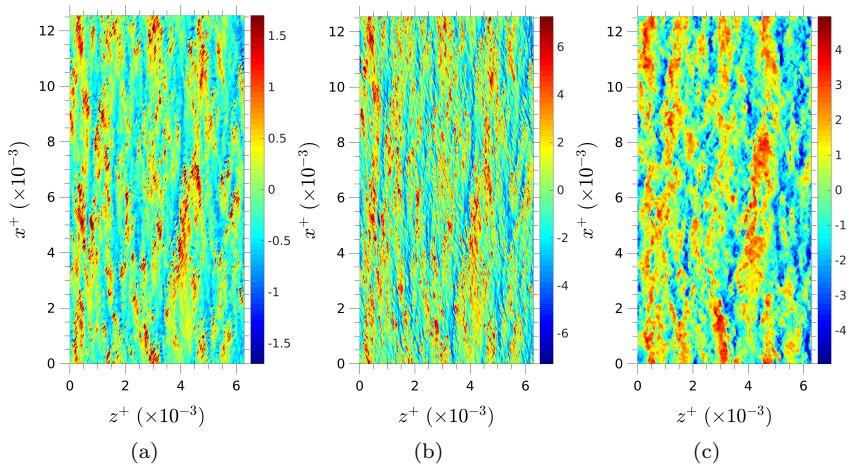


Fig. 1 Visual representation of the correlation between streamwise velocity fluctuations (u^+) at different wall-normal locations : (a) $y^+ \approx 3$ (surrogate of skin-friction field), (b) $y^+ \approx 18$ and (c) $y^+ \approx 200$. Note correspondence of large-scale regions of predominantly high- and low-velocity fluctuations. **Channel flow at $Re_\tau \approx 1000$ with oscillatory wall motion ($T^+ = 100$ and $A^+ = 12$).**

positive outer large-scale motions being much more pronounced than attenuation by negative large-scale footprints.

Very few studies undertaken so far deal, explicitly, with the impact of the large-scale motion, directly through foot-printing or indirectly through modulation, on the drag. de Giovanetti et al [15] have attempted to quantify the contribution of the large-scale motion by performing LES for canonical channel flow at Re_τ up to 4000 over domains of decreasing size, so as to progressively exclude large-scale motions in the outer region, estimating the contribution of the large-scale motion at around 20%. However, this conclusion has to be treated with caution as any undue restriction in the size of the computational box can readily lead to significant errors in the predicted drag level, even at very low Reynolds numbers (Quadrio (2017), private communication). On the other hand, Agostini and Leschziner [1] observed that large-scale footprints cause corresponding skin-friction fluctuations of order 15-20%, hence implying significant influence, even without an explicit account being taken of the effects of modulation.

The observation by Touber and Leschziner [39] and Blesbois et al. [9] that the drag-reduction level is linked closely to the ability of the spanwise Stokes strain to weaken the near-wall streaks and prevent their re-establishment strongly suggests that any mechanism or process that hinders the weakening of the streaks, and thus the quasi-streamwise vortices in the near-wall layer, is detrimental to the level of drag reduction achievable in ideal circumstances. Agostini and Leschziner [1,3] show that footprinting and modulation arising from outer structures are just such mechanisms, thus must be regarded as

primary candidate for affecting the drag-reduction effectiveness. It is precisely this interaction and its consequences that is at the center of the present study.

The study examines DNS data for a channel flow at $Re_\tau = 1020$ subjected to a streamwise homogeneous oscillatory spanwise motion at the near-optimum actuation period $T^+ = 100$. At this value, the observed mean drag-reduction level is 30% (Agostini et al [7]), and actuation-induced drag perturbations around the low-drag level are minimal, indicating that the time scale of the actuation is low enough to prevent the amplification of the streaks once they are weakened by the unsteady Stokes layer caused by the wall forcing.

2 The Database

The DNS data forming the basis of the analysis to follow herein were the subject of an earlier papers by Agostini et al [7,6], which focused on the physical processes associated with drag-reducing wall actuation. Therefore, only a brief statement of the main characteristics is given here.

The simulations were performed over a box of length, height and depth $4\pi h \times 2h \times 2\pi h$, respectively, corresponding to approximately $12 \times 2 \times 6 \times 10^3$ wall units. The box was covered by $1056 \times 528 \times 1056 (= 589 \times 10^6)$ nodes. The corresponding cell dimensions were $x^+, y^+_{min}, y^+_{max}, z^+ = 12.2, 0.4, 7.2, 6.1$. All simulations were progressed with a time-marching step chosen such that the CFL number did not exceed 0.25. The wall was actuated sinusoidally in spanwise direction according to $W(t) = W_m \sin(2\pi t/T)$ with period $T^+ = 100$ and 200, over a total period of $t^+ = 4600$ - thus corresponding to 46 actuation cycles at the lower period. Field variables were stored at intervals of $\delta t^+ \approx 10$.

The adequacy of the resolution is demonstrated in Agostini et al [7,6] by means of a comparison with a simulation of the unactuated flow over a grid of 1.2B cells, an examination of the resolved dissipation, relative to the imbalance of other terms in the turbulence-energy budget, an evaluation of the ratio of cell distances to the Kolmogorov length scale, and a comparison of the energy budget for the unactuated flow with the budget reported by Moser et al. [30] **for a Reynolds number similar to the present value.**

The question of whether the computational box is large enough to faithfully capture the large scales merits consideration. The large scales of interest here are those at $y^+ \approx 3.9\sqrt{Re_\tau}$, the position in the log layer at which the streamwise energy profile is elevated towards an outer plateau. Previous studies on canonical channel flow at $Re_\tau = 1000 - 5200$ (Lozano-Durán and Jiménez [24], lee and Moser [23] , Agostini and Leschziner [4]) show (or at least suggest) that the large-scale structures are separated in the spanwise direction by around $1 - 1.5h$, so that the present spanwise width of $6.3h$ can accommodate around 4-5 structures. This may be regarded as sufficient. On the other hand, the streamwise length scale of the structures can exceed $\lambda_x = 10h$, and this compares to the length of the computational box $L_x = 12.6h$. However, the most energetic struc-

tures are argued by Agostini and Leschziner [1,3] to have a length scale of around $\lambda_x \approx 8h$, and many of the structures have a length scale of $4000 - 6000$ wall units. Hoyas and Jiménez [16] (see also Jiménez [21]) argue that a representative limit of $\lambda_x \approx 10h$. Moreover, Lozano-Durán and Jiménez [24] show, on the basis of tests with different computational boxes, that the interaction between the large and small scales is correctly represented even if the domain is not large enough to capture the entire range of the large structures. Hence, it appears justifiable to assume that the large-scale structures contained in the computational box constitute a credible basis for quantifying the interactions at issue here.

3 Scale separation

The manner in which large scales and small scales are defined and separated is central to the characterisation of the interaction between them. There is no unique approach to this task, and there is, therefore, an inevitable degree of ambiguity in the separation process. The large majority of studies that rely on scale separation are based on Fourier filtering with prescribed cut-off wave-length values, based on features in the pre-multiplied spectra of the streamwise turbulence energy. In the most elaborate implementation by Zhang and Chernyshenko [44], the filter cut-off value is determined – or rather chosen - by reference to the Pareto front relating the large-scale-to-large-scale to the small-scale-to-small-scale correlation coefficients. The cut-off is then dictated by the (essentially arbitrary) choice of the large-scale and small-scale correlation coefficients – typically 0.9 and 0.1, respectively.

In contrast to the above Fourier-based approach, the route adopted herein entails a spatially two-dimensional extension of Huang et al's [17] *Empirical Mode Decomposition* (EMD). This method has previously been applied by Agostini and Leschziner [1,3,5,4] to the analysis of channel-flow data at $Re_\tau = 1020$ and 4200. The EMD has a number of attractive features that allows it to be used flexibly in the present context. The method splits any signal into a set of *Intrinsic Mode Functions* (IMFs) based purely on the local characteristic time/space scales. It requires no pre-determined functional elements, such as Fourier or wavelet functions. Rather, the IMFs are the EMD-generated basis functions, which arise purely from the given signal itself. Unlike Fourier methods, the EMD does not require filters to separate the scales, and does not involve filter-induced loss of energy. Thus, if the EMD is applied to a signal, the sum of the modes and the residual is identical to the parent signal [12,42]. In the particular case of a white noise, the sum of moments of the modes (e.g. variance) also yields the corresponding moments of the parent signal. However, this latter property does not apply to realistic turbulent signals. Importantly, a mode is not a signal having a unique frequency or length scale, but one that has a narrow range of scales and characterized by narrow-band spectrum with a mean scale that rises with mode count. An inherent property of the

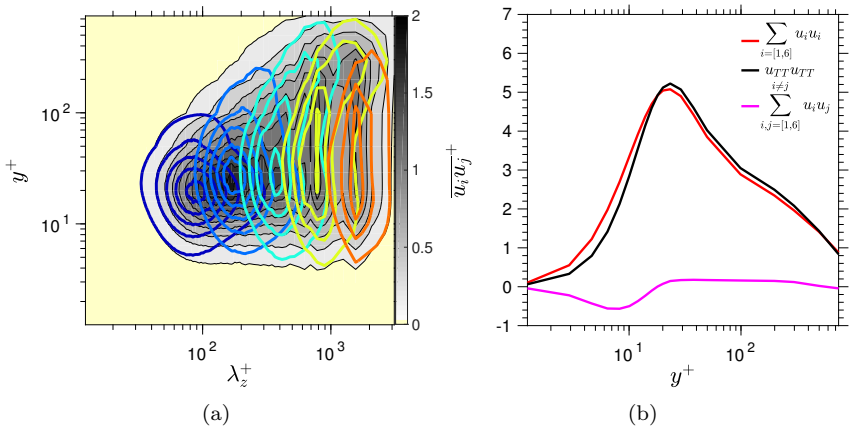


Fig. 2 EMD-mode decomposition of streamwise energy: (a) pre-multiplied spectra across the flow in terms of the spanwise wave length λ_z; grey contours represent the entire turbulence field, colour contours represent EMD modes $i = 1 - 5$; (b) Wall-normal distributions of the sum of the streamwise energy of EMD modes ($i = 1 - 6$) and cross-mode correlations ($i, j, i \neq j$) relative to the total streamwise energy.

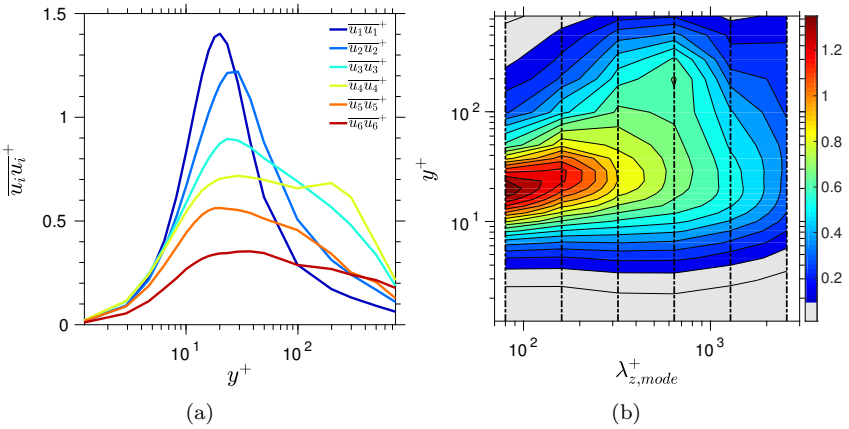


Fig. 3 Mode-wise contributions to the streamwise energy: (a) profiles of energy contributions from mode 1-6; (b) map of mode-by-mode energy profile, with modes identified by black vertical lines in terms of the wave lengths at which the respective premultiplied spectra of the modes reach their maximum value at $y^+ = 20$.

method is that the mean frequency and the bandwidth associated with each mode doubles between two successive modes [12].

Prior to analyzing the physical interactions between scales, based on a range of statistical indicators, the characteristics of the EMD in the present case of $Re_\tau = 1020$ and actuation period $T^+ = 100$ are illustrated in figures 2 to 4. Figure 2(a) shows the pre-multiplied spectra across the flow in terms of the spanwise wave length λ_z. The grey contours represent the entire turbulence field, while the coloured contours arise from EMD modes $i = 1 - 5$, (mode 6

is not visible simply because this mode contains an insignificant proportion of the total energy). Here, it is especially interesting to observe that all modes are highly coherent in the wall-normal direction, with even the largest-scale mode penetrating right down into the viscous sublayer. A quantitative description of the cross-flow correlation will be provided at the end of this section, in figure 4. Figure 2(b) illustrates that the energy components, derived from the EMD modes of the velocity signal, do not sum up to the respective total. The reason is that the total energy, $\overline{u_{TT}u_{TT}}$, consists of the mode-specific energy components and cross-mode correlations, $(\overline{u_i u_j} \neq 0, i \neq j)$, identified by the magenta line.

Figure 3 provides two different views of the contribution of the individual EMD modes to the streamwise energy $\overline{u'u'}$. **Figure 3(a) shows profiles of the energy components derived from modes 1-6 at $y^+ = 20$, this being the location at which the streamwise stress reaches its maximnum value (see figure 2). The map in figure 3(b) gives a composite view of the modal energy components in terms of y^+ and the wave lengths of the modes, the latter identified by the vertical black chain lines at wave-length values that correspond to the locations in figure 2(a) at which the spectra of the individual modes reach their respective maxima at $y^+ = 20$ – again, the location of the streamwise-energy peak.** Strictly, the correlation values in figure 3(b) are only relevant at the locations of the modes – i.e., at the discrete modal wave lengths, along the black lines. The continuous contour map thus arises from interpolating between the correlation levels along the lines identifying the modes, and this is done as a visual aid only. The most pertinent feature, in both plots 3(a) and 3(b), is the rise in mode 4 at $\lambda^+_{z,mode} \approx 650$ and $y^+ \approx 200$, which signifies most clearly the presence of large-scale outer motions . A second informative feature, consistent with comments made in relation to figure 2, is that the energy contribution of large-scale motion is substantial across the entire shear layer, including the buffer layer and the region below it - in effect, justifying the term "footprinting".

Figure 4 contains four maps that convey, in different ways, the level of streamwise variation of the correlation between the skin friction (C_f) and velocity modes or combination of modes. Given a velocity-fluctuation mode i, the two-point correlation coefficient $\mathrm{R}(\mathrm{y}^+, \Delta\mathrm{x}^+)$ is evaluated from:

$$R(y, \Delta x) = \frac{1}{N_t \times N_z} \sum_{k,l=1}^{N_t,N_z} \left(\frac{r_{12}(y, \Delta x, t_k, z_l)}{\sqrt{r_{11}(y, \Delta x, t_k, z_l)}.\sqrt{r_{22}(\Delta x, t_k, z_l)}} \right) \quad (1)$$

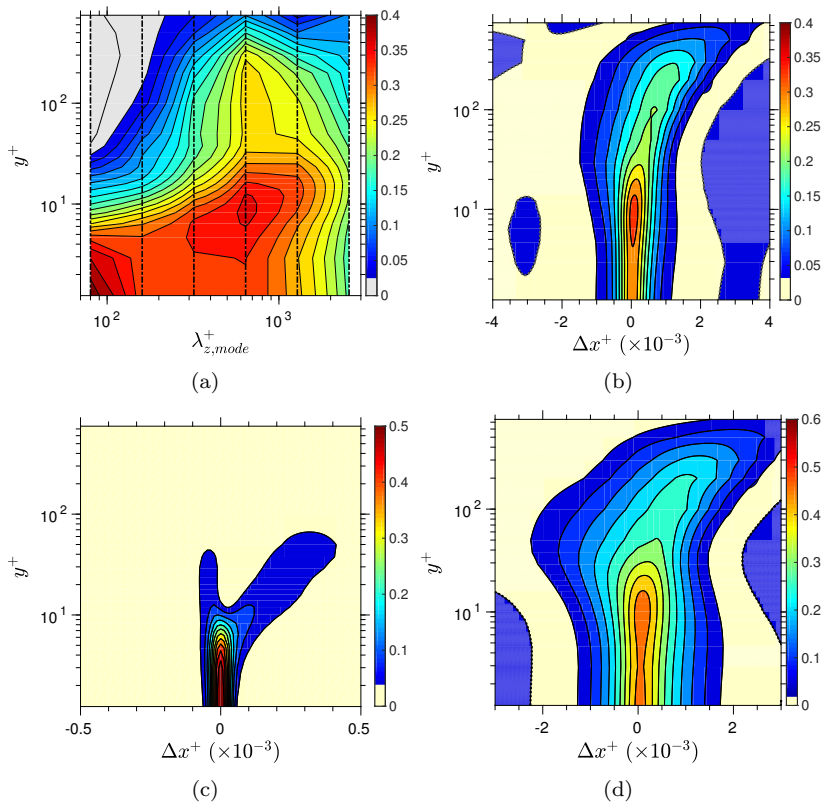


Fig. 4 Correlation-coefficient maps: (a) map of maximum correlation coefficient $R_{Cf,mode}(y^+, \Delta x^+)$ at any y^+ position of modes from 1 to 6 with Cf (black lines have the same meaning as in figure 3); (b) correlation map of C_f with the mode 4 ; (c) correlation map of C_f with the small-scale modes (1+2) and (d) correlation map of Cf with large-scale motions (modes 4+5+6).

where

$$r_{12}(y, \Delta x, t_k, z_l) = \sum_{i=1}^{N_x} [u_i(x_i + \Delta x, t_k, z_l) - < u_i(t_k, z_l) >_x] \times [Cf(x_i + \Delta x, y, t_k, z_l) - < Cf(y, t_k, z_l) >_x]$$

$$r_{11}(\Delta x, t_k, z_l) = \sum_{i=1}^{N_x} [u_i(x_i + \Delta x, t_k, z_l) - < u_i(t_k, z_l) >_x]^2$$

$$r_{22}(y, \Delta x, t_k, z_l) = \sum_{i=1}^{N_t} [Cf(t_i, y, t_k, z_l) - < Cf(y, t_k, z_l) >_x]^2,$$

and Δx^+ is the streamwise separation between the locations at which C_f and u_i are sampled.

Figure 4(a) shows a mode-by-mode map of R, with the black vertical lines having the same meaning as the lines in figure 3(b). Figures 4(b),(c) and (d) show, respectively, the correlation coefficients for mode 4, modes 1+2 – representing the small scales, and modes 4+5+6 – representing the large scales. This groupings reflect the view – or decision – that it is not appropriate to regard mode 3 as either a small-scale or large-scale mode. The rationale of this attribution is based on the spanwise wave-number location of the modal spectra shown in figure 2(a). The gray contours of the total field show the energy density to increase towards an outer maximum at $\lambda_z^+ \approx 700$. In contrast, mode 3 lies between the inner and outer maxima. **This mode is thus held to be an intermediate mode, which cannot be attributed to either the small-scale or large-scale sets of modes. In the following presentation and discussion, this mode is referred to as the *attached-eddy* (AE) mode. This designation gives expression to the fact that the intermediate mode is closely associated with the hierarchy of wall-attached eddies having particular statistical properties that comply with the attached-eddy hypothesis of Townsend [40] and Perry et al. [31]. This connection is described by Agostini and Leschziner [4] by reference to regions within the spectral maps for the streamwise fluctuations in a canonical channel flow at $Re_\tau = 4200$. The connection of the intermediate mode to the set of attached eddies is reflected, among other features, by the y^+-wise logarithmic decay of the energy of this mode, seen in figure 3(a), which is one statistical property that complies with the attached-eddy hypothesis** .

Figure 4 reveals a number of pertinent facts or features:

- The first two modes, associated with the small-scale structures (smaller than $\lambda_z^+ = 300$), are only correlated close to the wall, $y^+ < 50$. The shape of inverse lambda reflects a distinct hysteresis in the cycle of streak decay and generation during the periodic actuation cycle and the Stokes layer, an interaction that is discussed in detail by Agostini and Leschziner [7,6].

- Mode 4, of spanwise length scale, $\lambda_z^+ \approx 700$, is clearly exceptional, in so far as it reflects an enhanced link between large-scale motions at $y^+ \approx 200$ and the skin friction. However, the correlation coefficient at this wall-normal distance is around 0.25, and this is a rather modest value relative to the level observed in canonical (unactuated) channel flow at the same Reynolds number ([4]). There is a weak maximum, at around 0.35, in the correlation coefficient of mode 4 in the lower portion of the buffer layer. Both the modest correlation beyond the buffer layer and the maximum within it may be a consequence of the de-correlating influence of the unsteady transverse Stokes strain in the viscous sublayer. It is also possible that the peak in correlation is due, at least in part, to an asymmetric streak modulation by sweeps and ejections associated with positive and negative large-scale motions, respectively (an issue discussed in Section 4), and additionally to

the local generation of mode-4 energy that enhances the impact of scales at the wave length of mode 4 on the near-wall turbulence and the skin friction. A degree of support for the last supposition is provided by figure 3(a), which shows the mode-4 energy to be elevated in the buffer layer, relative to the energy at $y^+ > 100$.

– The composite correlation coefficient of modes 4-6, regarded as large-scale modes, shows a maximum correlation coefficient of approximately 0.35 at $y^+ \approx 200$, and the y-wise locus of the maximum features an inclination that characterizes a lag of order $\Delta x^+ \approx 1000$. This lag was highlighted already, in qualitative terms, by reference to figure 3(a). The S-shape of the correlation map is indicative, indirectly, of the eddies associated with modes 4-6 being detached, because the shape implies that perturbations are transmitted upwards only in the upper part of the near-wall layer and not from the wall. Here again, it is surprising, at first sight, to observe that the magnitude of the correlation coefficient is relatively low. However, it is informative to note here that a map (not included) of the correlation coefficient linking the large-scale component of C_f (modes 4-6) with the large-scale velocity fluctuations (modes 4-6) yields a correlation coefficient of about 0.6 at $y^+ \approx 200$.

It is finally instructive to refer here to figure 10 in Section 5, which conveys well the effect of the large-scale fluctuations on the small scales. This figure shows the fluctuation fields at $y^+ = 13$ reconstructed from modes 1+2 and mode 4+5+6, respectively. The main conclusion derived from this figure is that regions of elevated and depressed small-scale activity are visually well correlated with the regions of large-scale fluctuations – a relationship that reflects the process of modulation. The fact that the streaks are pronounced in regions of positive large-scale fluctuations, while they are virtually absent in regions of negative large-scale fluctuations is a first indication of substantial differences in the level of small-scale modulation within positive and negative large-scale footprints. These differences may be linked, in part, to the fact that large-scale footprints alter significantly the local level of the friction velocity u_τ, so that the wall-scaled period T^+ departs significantly from the optimum mean value $T^+ = 100$, thus favouring, locally, the recovery of the streaks during the actuation cycle.

4 Contribution of modes to the skin friction

With the above attribution of modes to the large-, intermediate- and small-scale fields established, it is possible to quantify the relative contribution of the three groups of modal motions to the skin friction. To this end, the Fukagata-Iwamoto-Kasagi (FIK) identity :

$$Cf = \frac{6}{Re_b} + 6\int_0^1 \left(1 - \frac{y}{h}\right)\left(-\frac{\overline{uv}}{U_b^2}\right) d\left(\frac{y}{h}\right) \tag{2}$$

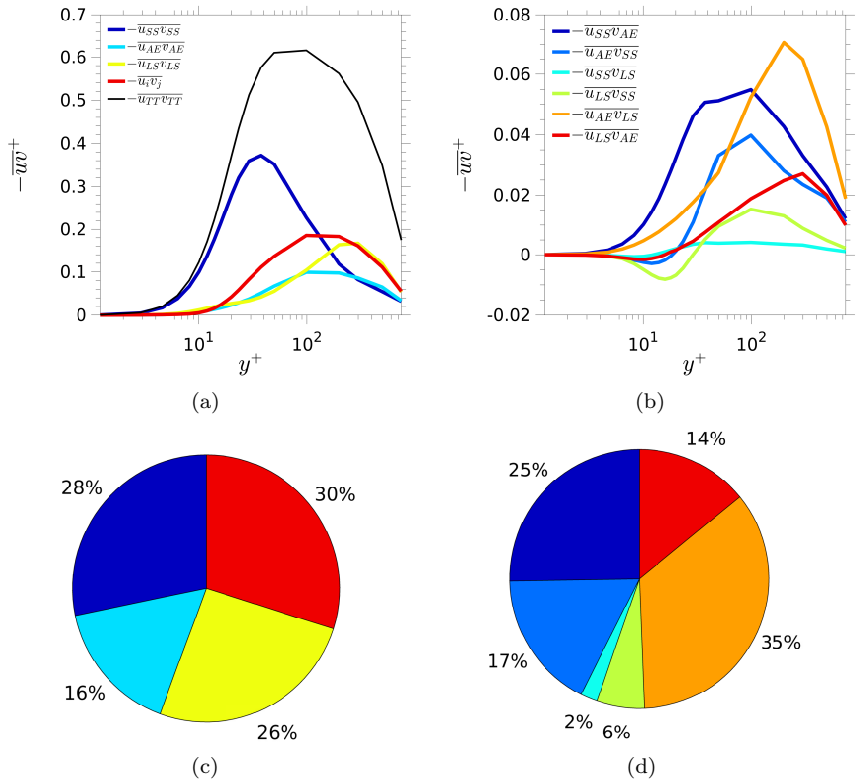


Fig. 5 Contributions of scales (SS-modes 1+2, LS-modes 4+5+6 and AE-mode 3) to the shear stress and skin friction C_f; (a,b) profiles of shear-stress fragments in equation 3; (c) contribution of the correlations in figure 5 (a) to the skin friction; (d) contribution of the individual inter-scale fragments $-u_iu_j$ to the sum of $-u_iu_j$.

may be used, in which the first term represents the viscous contribution, $Re_b = \frac{U_b h}{\nu}$ is the bulk Reynolds number, U_b is the bulk velocity and h is the channel half-height. The contributions to the shear stress may now be represented by

$$\overline{u_iv_j} = \begin{vmatrix} \overline{u_{SS}v_{SS}} & \overline{u_{SS}v_{AE}} & \overline{u_{SS}v_{LS}} \\ \overline{u_{AE}v_{SS}} & \overline{u_{AE}v_{AE}} & \overline{u_{AE}v_{LS}} \\ \overline{u_{LS}v_{SS}} & \overline{u_{LS}v_{AE}} & \overline{u_{LS}v_{LS}} \end{vmatrix} \tag{3}$$

and the fragments inserted into equation 2 , where AE stands for the attached-eddy mode 3, SS stands for modes 1+2 and LS stands for modes 4+5+6. The profiles of the shear-stress contributions in equation 3 are shown in Figure 5(a) and (b), the latter conveying the magnitude of the mixed terms $-\overline{u_iv_j}$, with $i \neq j$, **expressing interactions among the modes contributing to the respective correlations.**

The LS contribution to the skin friction is shown to be 26%, but the mixed mode contributions are also substantial, in contrast to the analogous fragments of streamwise energy, as will be shown below. In contrast to the above "direct" contribution of the LS modes, their "indirect" effect, via the modulation, cannot be determined by the $\overline{uv}$ scale decomposition, but the fact that $SS - LS$ cross-terms are finite suggests that the small-scale modulation is asymmetric. The AE mode makes an important contribution too, its direct contribution being 16%. Of the mixed-mode terms, those correlating small-scale and large-scale motions are relatively modest, but the variation of $\overline{u_{LS}v_{SS}}$ is especially interesting, in so far as this represents the modulating effect of the streamwise LS fluctuations on the wall-normal SS motions. The correlation is seen to be positive up to about $y^+ = 30$ and negative beyond this distance – i.e., it reduces the magnitude of the shear stress in the near-wall region and increases it outside the buffer layer. A qualitatively similar behavior is also observed in respect of the term $\overline{u_{LS}v_{AE}}$.

It is interesting to examine the consequence of including the AE mode either in the LS set or the SS set – that is, to regard the AE mode as being part of the large-scale or part of the small-scale field, respectively. The result of this alternative attributions is shown in figure 6. Thus, the inclusion of the AE mode in the LS set results in the LS contribution to C_f rising substantially, to 42%, relative to the level of 26% shown in figure 5, while the effect of including the AE mode in the SS field merely causes an increase in the relative contribution of the SS mode to C_f. In both cases, the contribution of mixed-mode fragments is small, as neither includes explicit correlations involving the AE mode.

The effect of attributing different sets of modes to the SS and LS contributions to the streamwise energy is shown in figure 7. Plots 7(a)-(c) correspond, respectively, to the results in figures 5 and 6. Thus, in figure 7(a), the AE mode is treated as a separate mode, while in figures 7(b) and (c), the AE mode is included in the LS and SS sets, respectively. In all three cases, the sum of the contributions is equal to the total streamwise energy. Also in all three cases, contributions other than the SS and LS sets are relatively minor, and this includes the relatively modest AE contribution when treated separately. Naturally, the inclusion of the AE mode in the LS set, figure 7(b), elevates the relative importance of the latter, while the inclusion of the AE mode in the SS set, elevates the SS profile.

A more differentiated view of the contribution of modes to the skin friction is given in figure 8 by way of streamwise spectra of skin-friction fluctuations. The spectrum of the total (raw) data is given by the black line and features two maxima, namely at $\lambda_x^+ \approx 150$ and 5000, the former associated with SS motions and the latter with LS footprints, thus illustrating the importance of the LS motions. Figure 8(a) shows, separately, the contributions of the SS, LS and AE modes. The sum of these three fragments is also shown by the blue line in figure 8(c), and this demonstrates that this sum is not the total. However, the inclusion of the mixed-mode terms, given by the red line, results in the total being correctly returned. The mixed-mode contributions

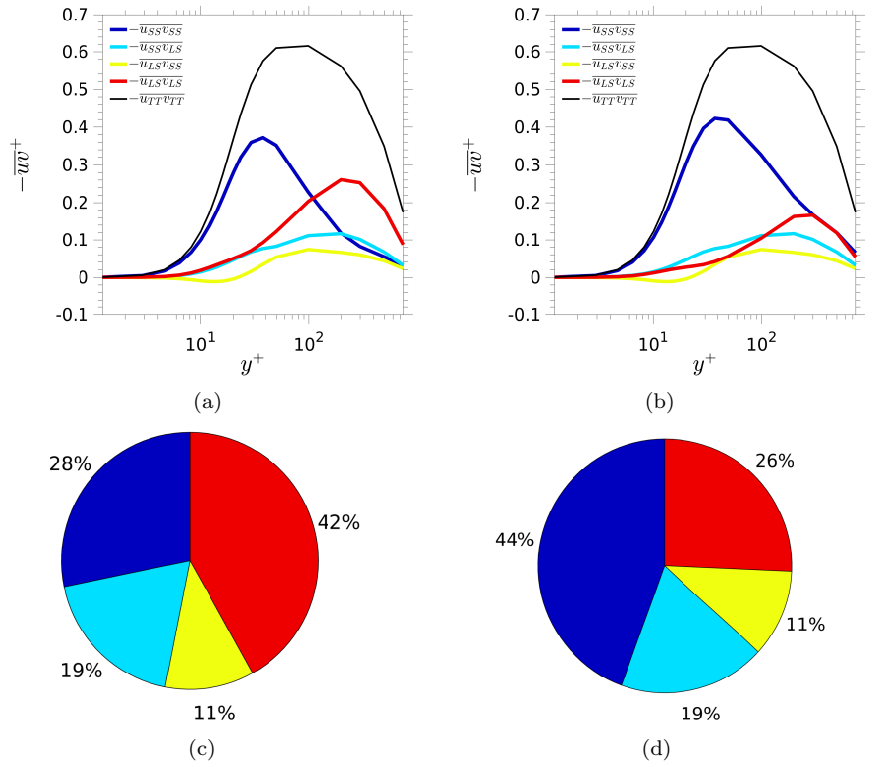


Fig. 6 Contributions of scales (SS-modes 1+2, LS-modes 4+5+6) to the shear stress and skin friction C_f subject to the intermediate AE mode 3 being attributed either to the LS set or the SS set; (a,c) profiles of shear-stress fragments and skin-friction contributions with the AE mode included in the LS set; (b,d) profiles of shear-stress fragments and skin-friction contributions with the AE mode included in the SS set.

conveyed by figure 8(b) is seen to be quite influential, and this is analogous to the important contribution made by corresponding mixed-mode terms to the shear-stress profiles in figure 5

A final statistical indicator used here to demonstrate the importance of the large-scales to the skin friction as well as its small-scale field is via PDFs of the total (TT), LS and SS fluctuations, normalized by the skin friction of the unactuated flow, **these contributions being derived from the EMD decomposition** $Cf_{TT} = Cf_{SS} + Cf_{AE} + Cf_{LS} + \overline{Cf}$. Such PDFs, the area underneath all four being unity, are shown in figure 9. The mean (centre of gravity) of the PDF of the raw data is 0.7, corresponding to the 30% drag-reduction achieved by the actuation. The LS motions are seen to cause large skin-friction fluctuations of order $\approx -30\%$ **to** $\approx +60\%$ **of the mean value,** and its PDF is significantly skewed, as is the PDF of the total fluctuations. The skewness signifies a lower incidence of strong positive fluctuations, associated with sweeps, relative to a larger incidence of weaker negative fluctuations,

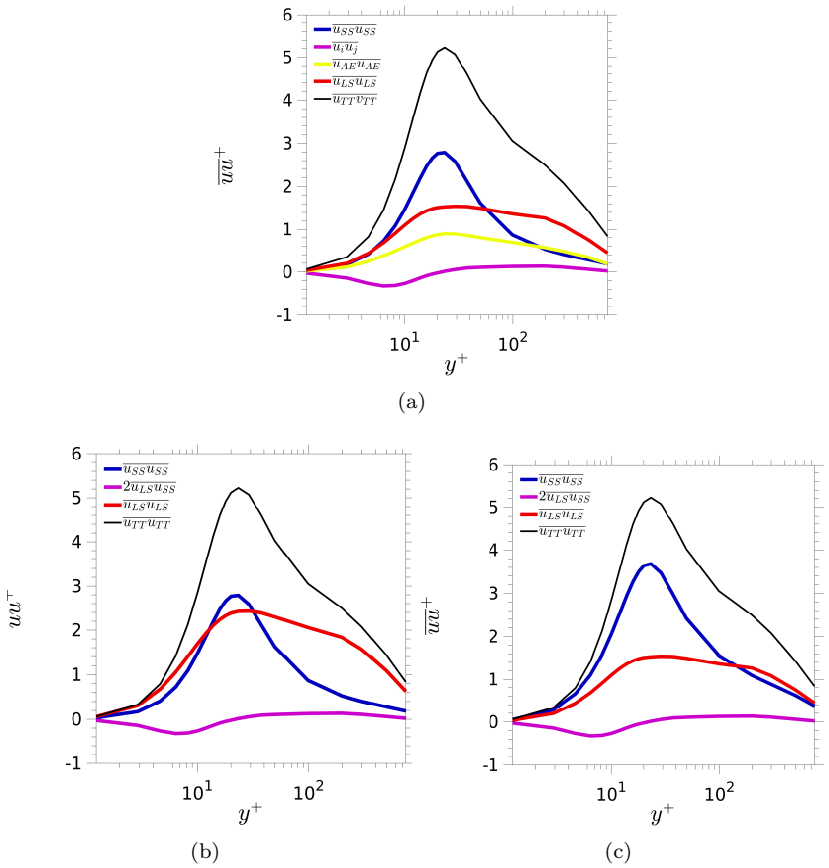


Fig. 7 Contributions of scales to the streamwise normal stress: (a) SS, LS and AE modes treated as separate; (b) AE mode included in the LS set; (c) AE mode included in SS set.

associated with ejections. **The joint $C_{f,SS} - C_{f,LS}$ PDF in figure 9(d) shows that the intensity and skewness of the SS fluctuations are both considerably larger for positive LS fluctuations than for negative ones, thus again pointing to a strongly asymmetric response of the modulation to the sign of the LS fluctuations.** Skin-friction fluctuations due to the SS modes are not much weaker, but the PDF of the SS set is only modestly skewed.

A result that give an interesting insight into the effects of the interactions between the LS and SS motions on the skin friction is the joint $Cf_{SS} - Cf_{LS}$ PDF shown in figure 9(d). A first conclusion derived from this plot is that SS fluctuations are significantly weaker in regions of negative LS fluctuations, while SS fluctuations tend to be substantially stronger in regions of positive LS fluctuations. This is a first indication a material asymmetry in the modulation of the SS fluctuation intensity (or energy) by the LS motions – a subject

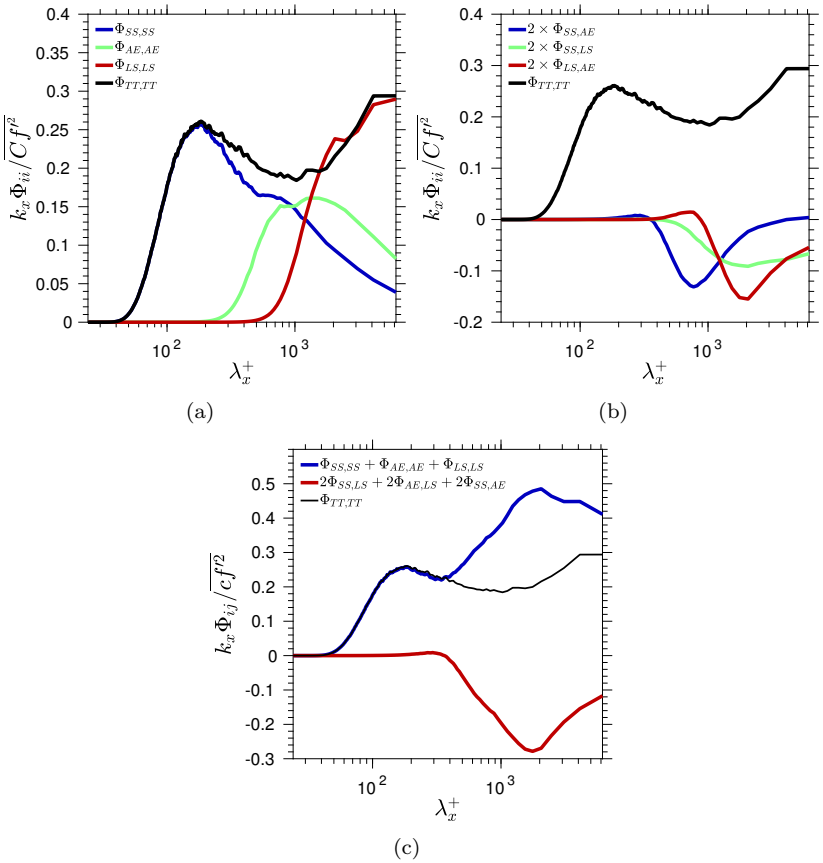


Fig. 8 Contributions of scales to streamwise skin-friction spectrum: (a) contribution of SS, LS and AE modes treated as separate; **(b) inter-scales contributions of SS, LS and AE modes and (c)** sum of principal (LS, SS, AE) contributions and mixed-mode contributions

that occupies a major proportion of the material presented in the next section. Second, there is a non-negligible correlation between SS and LS fluctuations: large positive LS fluctuations are associated, preferentially, with negative SS fluctuations, rather than positive ones. In other words, the 'local mean' of the SS fluctuations is predominantly negative in the presence of positive LS fluctuations. This suggests an increasing level of skewness in the SS fluctuations when this is conditioned on large positive LS fluctuations, thus increasing the asymmetry in the modulation.

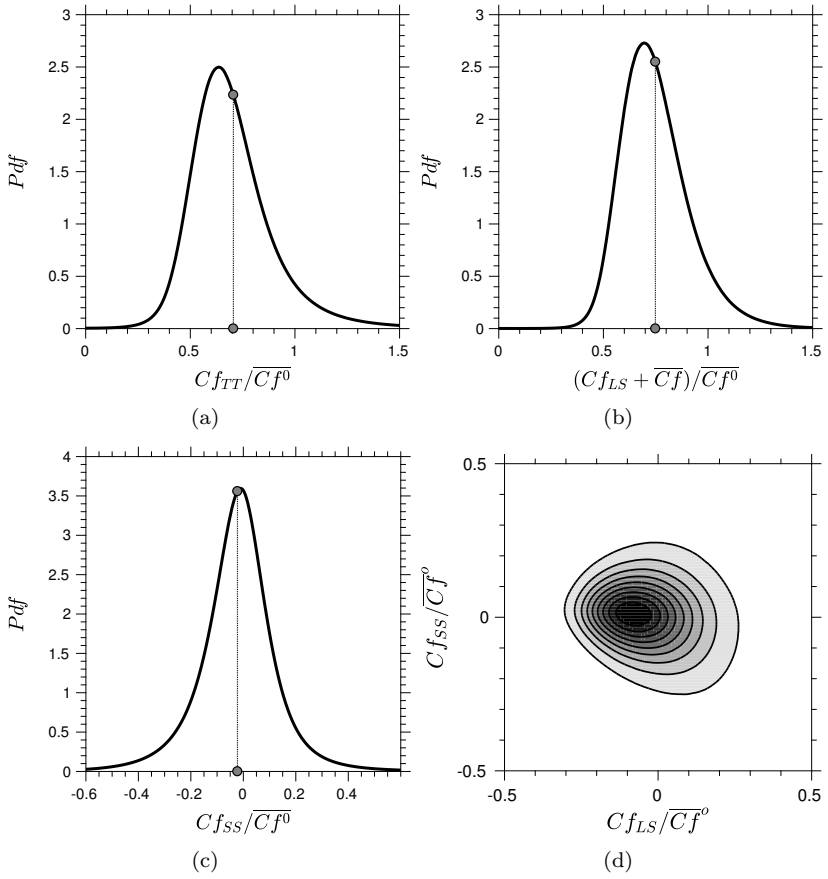


Fig. 9 PDFs of skin-friction fluctuations: (a) total (raw) data; (b) LS contribution; (c) SS contribution and (d) joint PDF of SS and LS skin-friction fluctuations.

5 Effects of large scales on small scales

5.1 Conditional statistics

In order to extract statistical data that provide insight into the interactions between the large outer and small inner scales, statistics are derived from the SS velocity fluctuations conditioned on regions of high-velocity, low-velocity, and near-zero LS footprints. Regions of high-velocity and low-velocity LS motions are defined here as those which fall into a chosen portion (5%, 10%, etc.) of the lowest and highest motions within the PDF of the entire LS field, while regions which are, essentially, devoid of LS footprints are defined as those which fall into a selected central portion of the PDF. This is illustrated in figures 10(a) and (b), which exemplify, respectively, sampled patches within the fields of LS and SS motions, subject to a condition level of +5%.

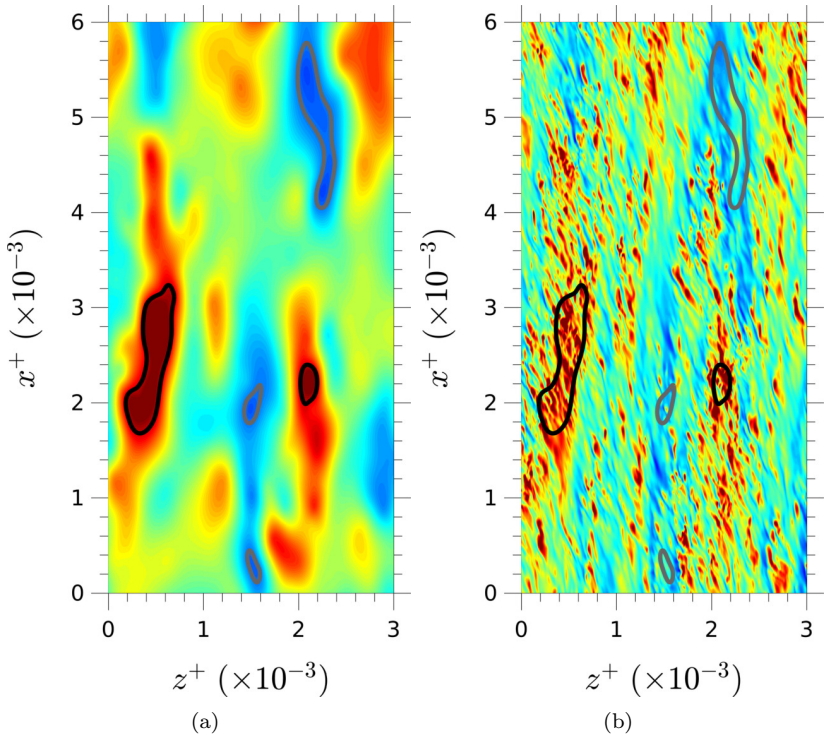


Fig. 10 Illustration of the conditional sampling and averaging process for small-scale properties within defined portions of large-scale footprints; (a) LS field, (b) raw field, both at $y^+ = 13$.

It needs to be emphasized that there is no fundamentally profound reason for any particular choice of the bands in the LS PDF within which SS motions are sampled. A choice of 5% or 10%, say, is motivated by the wish to bring out as clearly as is possible differences in the effects of positive and negative LS fluctuations on the SS motions. Increasing the conditional limit weakens these differences, but does not change the nature of the message, as will be shown below.

Figure 10 conveys the fact that the streaky structure – the inclined densely-spaced lines — are rather weak in regions of low LS motions, due to the fact that the near-optimum wall actuation (in the mean) substantially depresses the streamwise energy in the buffer layer. The streaks are evidently amplified by positive LS footprints. This type of amplification – or positive modulation – is also observed in canonical (uncontrolled) channel flow [1,2], but the effect may be accentuated, as already conjectured at the end of Section 3, by the fact that the locally elevated wall shear stress leads to locally non-optimum values of the wall-scaled actuation period $T^+ = Tu_\tau^2/\nu$ (note the quadratic dependence on u_τ).

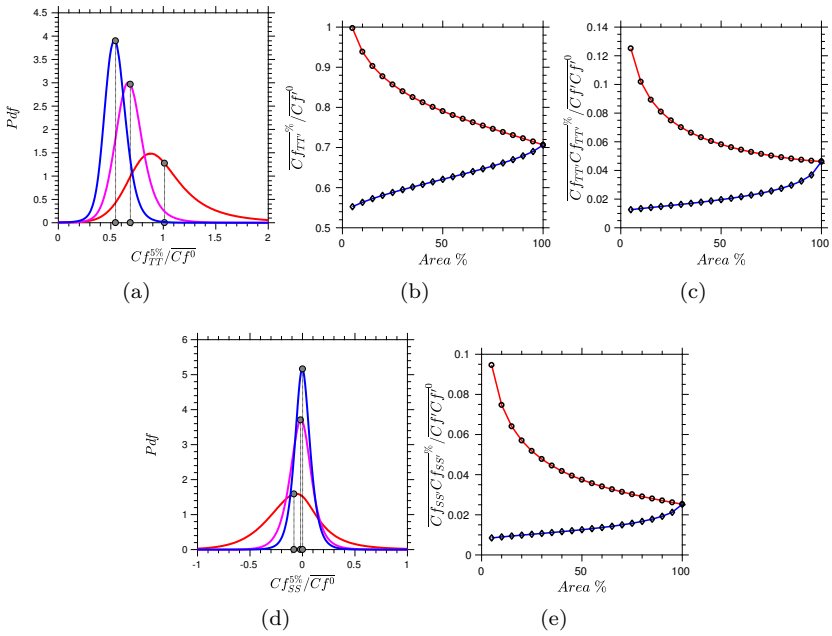


Fig. 11 PDFs of skin-friction fluctuations: (a) PDFs of total fluctuations conditional on extreme 5% of large-scale fluctuations (red and blue profiles) and on 5% regions of lowest large-scale fluctuations (purple profile); (b) variation of mean skin friction (centres of gravity of PDFs in (a)) in regions of extreme large-scale fluctuations as a function of the condition, $Area = 5 - 100\%$, imposed on extreme large-scale fluctuations (5-100%); (c) variation of variance of PDFs in (a) subject to same conditions as (b); (d) PDFs of small-scale skin-friction fluctuations subject to same conditions as (a); ; (e) variation of variance of small-scale fluctuations subject to same conditions as (c).

5.2 Properties of skin-friction fluctuations within footprints

In order to gain a more detailed, quantitative, view of the effects of the footprints on the skin-friction, conditional PDFs for the total skin-friction, Cf_{TT}, and small-scale skin-friction fluctuations, Cf_{SS}, were assembled in patches characterized by (i.e., conditioned on) prescribed limits of large-scale footprints.

Figure 11(a) and (d) each shows three PDFs for Cf_{TT} and Cf_{SS}, respectively, two within regions conditioned on 5% positive and negative LS fluctuations and the third within the central 5% region in which the LS motions are weakest. All distributions are normalized by the mean skin-friction value of the unactuated flow, i.e. 1/0.7 of the actuated case. The vertical black lines indicate the centres of gravity of the respective PDFs – i.e., in the case of Cf_{TT} in figure 11(a), the mean value of the skin friction is 0.7. Figure 11(b) and (c) show, respectively, the variations of the centers of gravity of the PDFs for the extreme positive and negative LS fluctuations and the variance of the PDFs as the value LS condition is progressively increased from 5% to 100% (identified

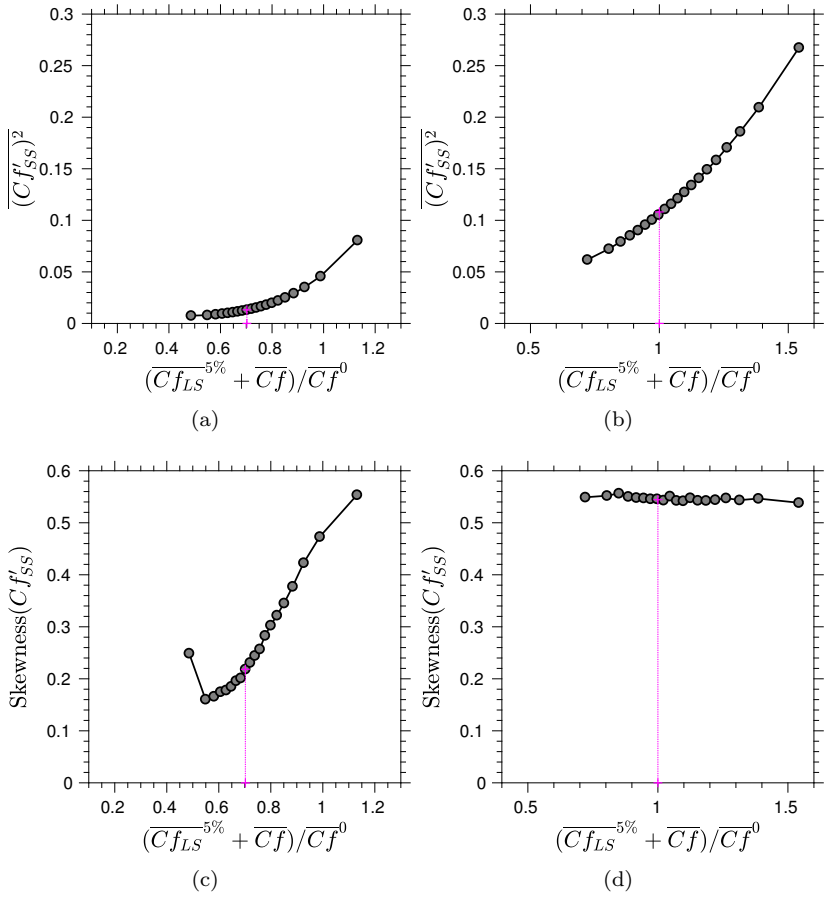


Fig. 12 Asymmetric response of SS skin-friction fluctuations to the LS footprints: (a) variance for actuated flow; (b) variance for unactuated flow; (c) skewness for actuated flow; (d) skewness for unactuated flow. The circles indicate the centres of the 5% slivers of the LS PDF for the skin-friction fluctuations within which the SS PDFs have been determined. The verical magenta lines indicate the average drag level, relative to the unactuated-flow value.

by $Area\%$), the latter representing the non-conditioned overall mean. Figure 11(e) pertains to the Cf_{SS} fluctuations and correspond to 11(c).

A first conclusion emerging from the figure is that skin-friction fluctuations are extremely high, especially within regions of high positive LS fluctuations. Thus, skin-friction fluctuations within regions of highest LS footprints exceed 100% of the overall average value. Moreover, the mean Cf_{TT} value within the extreme positive 5% LS fluctuations is about 30% higher than the average, while the standard deviation reaches 35% (the variance being 0.13). A second observation is that the variance of the PDFs, essentially representative of the intensity of the small-scale motions, differs greatly for positive and negative

LS fluctuations, the variance associated with positive footprints being much larger. In other words, the modulation of the small-scale motions and skin-friction fluctuations is highly asymmetric. This is, thus, a quantitative confirmation of the qualitative observations made in Section 5.1, by reference to figure 10, and also Fig. 9(d) in Section 4 - namely, that positive LS footprints cause (or are associated with) with a substantial amplification of small-scale activity, while negative footprints only cause weak attenuation of the SS fluctuations, which are already weak because of the actuation. Attention is drawn to the fact that the variance of the PDF for Cf_{SS}, figure 11(b), is similar to that of the Cf_{TT} PDFs, thus justifying the earlier assertion that the shape of the PDFs of the total fluctuations is essentially representative of those for the SS fluctuations.

In figure 11, it is shown that increasing the LS condition value – i.e. increasing the tail regions of the LS PDF in which SS fluctuations are sampled – results in a progressive convergence of the variance values of the PDFs for positive and negative LS fluctuations, ending with a single value that represents the mean state. In order to examine more closely the properties of SS PDFs within the range of LS fluctuations, the LS skin-friction PDF is divided into 5% sub-ranges or *slivers*. **Within each sliver, the SS variance and skewness are determined. The results are shown in figure 12, in comparison to corresponding results for the unactuated (canonical) flow at the same Reynolds number. The superscript 5% in the abscissa signifies the mean value of Cf_{LS} in the sliver in question, and the magenta lines indicate the overall mean value of the skin friction for both cases, respectively. The left-most value in all four figures pertain to the extreme negative tail of the LS PDF, i.e. the condition -5%, while the right-most value pertains to the extreme positive LS PDF condition +5%.**

As regards the variance, the overall level in the actuated flow is much lower than in the canonical flow, and this simply reflects the much lower intensity of the small-scale turbulence (including the streaks) in the buffer and viscous sublayers. In both cases, the variance rises substantially with increasing LS intensity, but the *rate* of increase is much steeper in the actuated case: the variance rises steeply for increasing positive LS skin-friction fluctuations and declines modestly for negative LS fluctuations, thus demonstrating the fact that, in this actuated case, the response of the small-scale turbulence to the LS motion is much more asymmetric with respect to the sign of the LS fluctuations, relative to close-to-linear variation in the canonical flow. An even more striking reflection of the asymmetric response to the LS fluctuations emerges from the comparison of the skewness distributions. In the canonical case, the skewness is almost constant, while it increases progressively with increasing LS intensity from a very low level at negative LS fluctuations, in which case turbulence is low, the streaks are very weak and turbulence is close to Gaussian. The positive skewness at large positive LS fluc-

tuations is well brought out by the PDF in figure 11 and is also consistent with the skewed features of the joint PDF in figure 9(d). The increasingly positive skewness arises in combination with large-scale sweeping motions, and this tends to transport high-intensity SS energy from the buffer layer towards the wall, thus favouring high positive SS fluctuations, relative to negative fluctuations that are associated with ejections. Hence, the asymmetric response of the SS field to the LS fluctuations structures is given expression by the width as well as shape of SS PDFs.

5.3 Conditioned velocity and stress distributions

Figure 13 shows conditioned viscous as well as turbulent shear-stress distributions and streamwise-energy profiles, subject to the same three different conditioning limits adopted in figure 11(a) – namely, the extreme 5% tails of the LS PDF and the 5% middle slice of the PDF. Here again, each plot contains three distributions per quantity, corresponding to those in figure 11(a). Figures 13(a) and (b) show profiles of the *total* stresses, sampled from the total fluctuations recorded in the conditioned patches, while figures 13(c) and (d) contain only the SS turbulent stresses. The viscous stresses have, obviously, to asymptote to the wall shear stress, and the asymptotic values correspond exactly to the C_f curves in figure 11(a). As regards the *total* turbulent-stress profiles, it is important to point out first that a consequence of the conditional sampling is that these do not include the full contribution of large-scale fluctuations. **This is because the *total* stresses in figure 13(a)(b) are derived, intentionally, within the narrowly defined regions of large-scale fluctuations, in which case the statistics are not sensitive to contributions associated with the large-scale fluctuations themselves.** In particular, when this limit is tight, the contribution of large-scale motions to the turbulent shear stress is excluded, and so are any contributions that arise from the correlation between large-scale and small-scale motions. What *is* included, in contrast to the SS stresses, shown in figure 13(c), are the motions represented by intermediate mode 3, and this is the main reasons for the difference between the stresses in figures 13(a)(b) and 13(c)(d) . All figures show that positive LS fluctuations provoke a 'shift' of the turbulent-stress profile towards the wall, leading to a material thinning of the viscous sublayer. The opposite occurs in regions in which the LS fluctuations are negative. The overall result is a strong increase or decrease in the turbulence activity close to the wall and hence commensurate consequences to the skin friction. In agreement with earlier observations the effects of positive and negative LS fluctuations is asymmetric, with positive fluctuations exerting a materially stronger effect on the stresses. Remarkably, the maxima of the shear-stress profiles are only weakly sensitive to the sign and intensity of the LS motions. In contrast, the streamwise-stress maxima, associated with the streaks in the buffer layer, are significantly more sensitive to the LS fluctuations, which accords with earlier

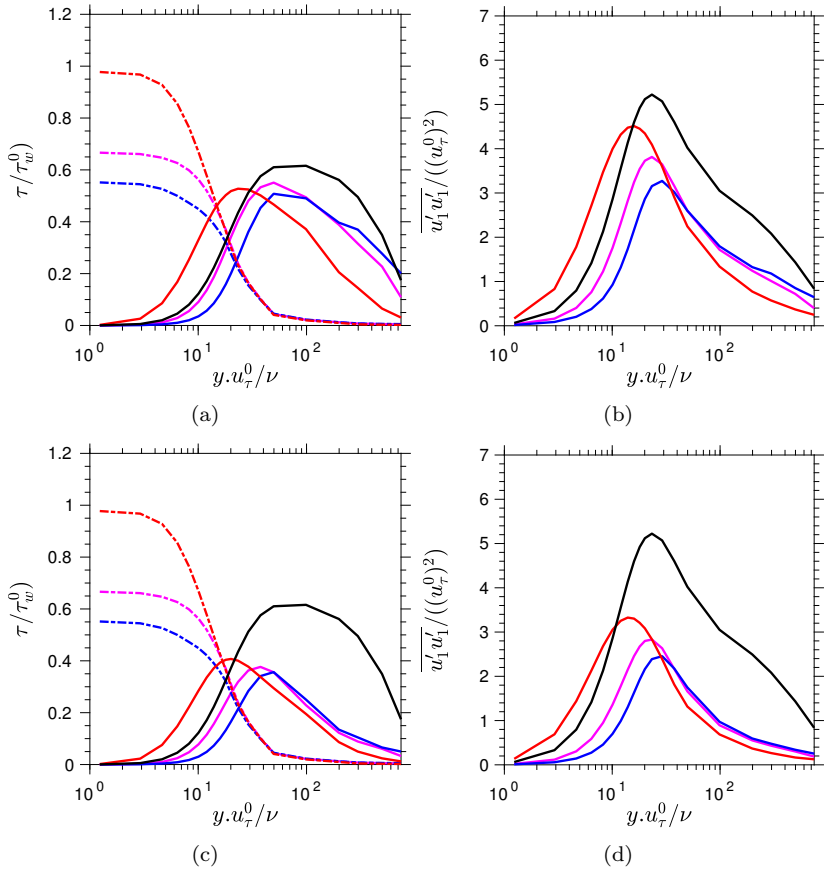


Fig. 13 Stress profiles conditioned on the extreme positive and negative and weakest 5% *LS* events,**represented in red, blue and magenta, respectively** ; (a) viscous and turbulent shear stresses derived from the total fluctuations in the sampled patches; (b) normal stresses derived from the total fluctuations in the sampled patches; (c) as (a), but derived from the *SS* fluctuations only; (d) as (b), but derived from the *SS* fluctuations only. **The black lines show the stress profiles obtained from the total field.**

observations relating to modulation. The wall-normal shift in the maxima, rather than a significant change in the level of the stresses, may reflect the convective-transport role played by *LS* sweeps (in the case of positive *LS* fluctuations) and ejections (in the case of negative *LS* fluctuations). As an aside, it is remarked that an examination of the pre-multiplied derivative of the second-order structure function, which is a surrogate of the energy spectra [40,11,4], not included herein, reveals a distinctive shift of the entire turbulence-intensity field towards or away from the wall when the *LS* fluctuations change sign.

A question that has been addressed by several past studies [25,44,2] on canonical channel flow is whether scaling with the *LS*-induced wall shear stress leads to a universal form of the near-wall *SS* turbulence statistics, referred to as

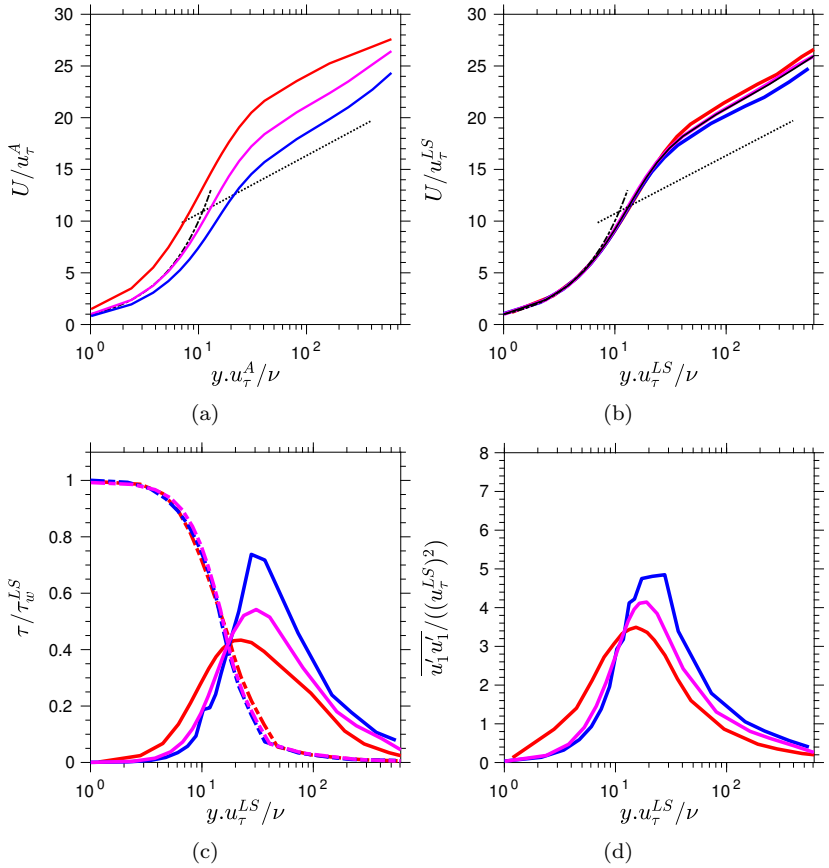


Fig. 14 Examination of Quasi-Steady concept by reference to velocity and SS shear-stress profiles conditioned on 5% limits on the LS motions: (a) velocity log law scaled with average wall shear stress of actuated flow; (b) as (a), but scaled with local LS-modified wall shear stress; (c) as figure 13(c) but with local LS scaling; (d) as figure 13(d), but with local LS scaling.

a *Quasi-Steady Hypothesis* and suggesting that the small-scale field responds instantaneously to large-scale footprints. The consequences of such "local" scaling are examined in figure 14. This shows, for the same conditions as in figure 13, the velocity log-law, the SS shear-stress profiles and the SS normal-stress profiles, all scaled with the LS-modified wall-shear stress that prevails in the conditionally sampled patches. Also included, in figure 14(a), is the log-law scaled with the average wall shear stress of the *actuated* flow. The upward shift in the log law is characteristic of the drag-reducing effect of the wall actuation. While it is evident from figure 14(b) that local scaling aides the collapse of the velocity profiles, the stress profiles do not comply with the quasi-steady concept. Local scaling is seen to have diminished the wall-normal

displacement of the stress maxima, but the stresses associated with positive LS fluctuations encroach onto the viscous sublayer, thus implying a detrimental impact on the drag. As the turbulent profiles represent the small-scale motions, the implication is that this encroachment is primarily a consequence of strong modulation that prevents the small-scale field from responding to the positive LS fluctuations in a quasi-steady manner.

The inapplicability of the QSH, demonstrated above for the actuated case, is also given expression by the behaviour shown in figure 12. The fact that the variance in the canonical case responds almost linearly to the LS intensity, while the skewness remains almost constant, points to the QSH being valid for that case, at least close to wall, as demonstrated by Agostini and Leschziner [2], albeit at $Re_\tau = 4200$. In contrast, as argued by reference to figure 14, the QSH does not hold for the actuated flow, and in this case, the small-scale structure responds non-linearly and in a much more complex fashion to the LS fluctuations.

6 Concluding Remarks

The ultimate objective of analyzing the interaction between outer large scales and the near-wall turbulence structure, in the present context of drag-reduction by wall actuation, is to quantify the effects of the outer structures on the skin-friction and possibly on the effectiveness of its reduction by the active skin-friction control. This is only possible to a limited extent with the application of statistical tools to a single flow. Ultimately, a full quantitative statement is only likely to emerge by a direct implementation of measures in simulations that are specifically designed to suppress the outer structures. Notwithstanding the above limitations, it may be argued that the present study has highlighted some important processes that are caused by the outer structures and identified material effects of these structures on the near-wall mechanisms and thus the skin friction.

An influential issue in the present statistical analysis is the manner in which scales, or scale ranges, are defined as being either “large” or “small”. The present EMD scale-separation method led to the conclusion that certain intermediate scales, interpretable as attached eddies, should be excluded from either the set of modes constituting the small scales or those defining the large scales. This decision is shown to be influential especially in respect of quantifying the direct contribution of the large scales to the turbulent shear stresses and thus the skin friction. With the attached-eddy scales excluded or included in the set of large scales, the contributions of the large scales to the total skin friction are 26% and 42%, respectively. This juxtaposition aside, the attached-eddy scales were excluded from the set of large scales, especially in the conditional statistics that constitute the principal pillar of this study..

The main observations and conclusions arising from the study may be summarized as follows:

- The EMD analysis has identified that large-scale motions in the log layer, at around $y^+ \approx 200$ and spanwise length scales of $\lambda_z \approx 650$, are preferentially correlated with the skin friction. The value of the correlation coefficient, at around 0.25, is modest relative to that in a canonical channel flow at the same Reynolds number, but this is highly likely to reflect the de-correlating influence of the periodic actuation and unsteady Stokes layer. The correlation maps for the large-scale motions show a spanwise lag of approximately 1000 wall units, relative to the skin friction, which is broadly in line with observations in canonical channel flows.
- Skin-friction fluctuations can exceed 100% of the overall mean value, as a combined consequence of the large-scale motions (footprints) themselves and the effect of the large-scale motions on the small scale field. Large-scale skin-friction fluctuations, on their own, are of the order 30% of the overall mean.
- There is irrefutable evidence of positive large-scale motions (or footprints) causing a substantial amplification of the near-wall turbulence – the streaks, in particular – and thus commensurate increase in small-scale skin-friction fluctuations, manifested by large values of the variance of the PDFs of small-scale skin-friction fluctuations. This suggests, on its own, a deleterious influence on the drag-reduction effectiveness of the actuation, although the level cannot be stated in quantitative terms.
- There is a strong asymmetry in the effects of positive and negative large scales on the near-wall conditions: positive large-scale motions are more intense and cause far more intense amplification of the small scales than the mild attenuation caused by negative large-scale motions. The observation of this asymmetry arguably increases the likelihood of adverse effects on the drag and the processes responsible for the drag reduction.
- A consequence of positive large-scale motions is a substantial thinning of the viscous sublayer **and, associated with it,** a substantial increase in the wall shear stress. Conversely, negative large-scale motions cause a more modest increase in the thickness of the viscous sublayer and modest decrease in the wall shear stress. This is, again, part and parcel of asymmetric response of the near-wall conditions to positive and negative large-scale motions.
- The limited examination of the *Quasi-Steady Hypothesis* of the velocity and small-scale shear and streamwise stresses indicates that the concept applies fairly well to the velocity, but is not valid for the stresses. This applies especially to the small-scale stress in regions of high positive large-scale fluctuations.

Acknowledgements

The research reported in this paper was undertaken within the framework of the EU-China project DRAGY, Grant Agreement 690623.

Disclosure statement

The authors declare that they have no conflict of interest.

References

1. Agostini, L., Leschziner, M.: On the influence of outer large-scale structures on near-wall turbulence in channel flow. Physics of Fluids **26**(7), 075,107 (2014)
2. Agostini, L., Leschziner, M.: On the validity of the quasi-steady-turbulence hypothesis in representing the effects of large scales on small scales in boundary layers. Physics of Fluids **28**(4), 045,102 (2016)
3. Agostini, L., Leschziner, M.: Predicting the response of small-scale near-wall turbulence to large-scale outer motions. Physics of Fluids **28**(1) (2016)
4. Agostini, L., Leschziner, M.: Spectral analysis of near-wall turbulence in channel flow at Re = 4200 with emphasis on the attached-eddy hypothesis. Physical Review Fluids **2**(1) (2017)
5. Agostini, L., Leschziner, M., Gaitonde, D.: Skewness-induced asymmetric modulation of small-scale turbulence by large-scale structures. Physics of Fluids **28**(1), 015,110 (2016)
6. Agostini, L., Touber, E., Leschziner, M.: The turbulence vorticity as a window to the physics of friction-drag reduction by oscillatory wall motion. International Journal of Heat and Fluid Flow **51**, 3–15 (2015)
7. Agostini, L., Touber, E., Leschziner, M.A.: Spanwise oscillatory wall motion in channel flow: drag-reduction mechanisms inferred from DNS-predicted phase-wise property variations at. Journal of Fluid Mechanics **743**, 606–635 (2014)
8. Bernardini, M., Pirozzoli, S.: Inner/outer layer interactions in turbulent boundary layers: a refined measure for the large-scale amplitude modulation mechanism. Physics of Fluids **23**(6), 061,701 (2011)
9. Blesbois, O., Chernyshenko, S.I., Touber, E., Leschziner, M.A.: Pattern prediction by linear analysis of turbulent flow with drag reduction by wall oscillation. Journal of Fluid Mechanics **724**, 607–641 (2013)
10. Chung, Y.M., Hurst, E., Yang, Q.: DNS for Turbulent Drag Reduction at Re_τ = 1600. In: Y. Zhou, A. Lucey, Y. Liu, L. Huang (eds.) Fluid-Structure-Sound Interactions and Control, pp. 145–149. Springer Berlin Heidelberg, Berlin, Heidelberg (2016)
11. Davidson, P., Krogstad, P.A., Nickels, T., others: A refined interpretation of the logarithmic structure function law in wall layer turbulence. Physics of Fluids **18**(6), 5112 (2006)
12. Flandrin, P., Rilling, G., Goncalves, P.: Empirical mode decomposition as a filter bank. Signal Processing Letters, IEEE **11**(2), 112–114 (2004)
13. Gatti, D., Quadrio, M.: Performance losses of drag-reducing spanwise forcing at moderate values of the Reynolds number. Physics of Fluids **25**(12), 125,109 (2013)
14. Gatti, D., Quadrio, M.: Reynolds-number dependence of turbulent skin-friction drag reduction induced by spanwise forcing. Journal of Fluid Mechanics **802**, 553–582 (2016)
15. de Giovanetti, M., Hwang, Y., Choi, H.: Skin-friction generation by attached eddies in turbulent channel flow. Journal of Fluid Mechanics **808**, 511–538 (2016)
16. Hoyas, S., Jimnez, J.: Scaling of the velocity fluctuations in turbulent channels up to Re= 2003. Physics of fluids **18**, 011,702 (2006)
17. Huang, N.E., Shen, Z., Long, S.R., Wu, M.C., Shih, H.H., Zheng, Q., Yen, N.C., Tung, C.C., Liu, H.H.: The empirical mode decomposition and the Hilbert spectrum for nonlinear and non-stationary time series analysis. Proceedings of the Royal Society of London. Series A: Mathematical, Physical and Engineering Sciences **454**(1971), 903–995 (1998)
18. Hurst, E., Yang, Q., Chung, Y.M.: The effect of Reynolds number on turbulent drag reduction by streamwise travelling waves. Journal of Fluid Mechanics **759**, 28–55 (2014)
19. Hutchins, N., Monty, J.P., Ganapathisubramani, B., Ng, H.C.H., Marusic, I.: Three-dimensional conditional structure of a high-Reynolds-number turbulent boundary layer. Journal of Fluid Mechanics **673**, 255–285 (2011)

20. Hutchins, N., Nickels, T.B., Marusic, I., Chong, M.: Hot-wire spatial resolution issues in wall-bounded turbulence. Journal of Fluid Mechanics **635**, 103–136 (2009)
21. Jimnez, J.: Near-wall turbulence. Physics of Fluids **25**(10), 101,302 (2013)
22. Lardeau, S., Leschziner, M.A.: The streamwise drag-reduction response of a boundary layer subjected to a sudden imposition of transverse oscillatory wall motion. Physics of Fluids **25**(7), 075,109–17 (2013)
23. Lee, M., Moser, R.D.: Direct numerical simulation of turbulent channel flow up to $Re_\tau=5200$. Journal of Fluid Mechanics **774**, 395–415 (2015)
24. Lozano-Durn, A., Jimnez, J.: Effect of the computational domain on direct simulations of turbulent channels up to Re= 4200. Physics of Fluids **26**(1), 011,702 (2014)
25. Lozano-Durn, A., Jimnez, J.: Time-resolved evolution of coherent structures in turbulent channels: characterization of eddies and cascades. Journal of Fluid Mechanics **759**, 432–471 (2014)
26. Luchini, P.: Reducing the turbulent skin friction. In: ECCOMAS conference on numerical methods in engineering, pp. 465–470 (1996)
27. Marusic, I., Mathis, R., Hutchins, N.: Predictive model for wall-bounded turbulent flow. Science **329**(5988), 193–196 (2010)
28. Mathis, R., Hutchins, N., Marusic, I.: Large-scale amplitude modulation of the small-scale structures in turbulent boundary layers. Journal of Fluid Mechanics **628**, 311–337 (2009)
29. Mathis, R., Monty, J.P., Hutchins, N., Marusic, I.: Comparison of large-scale amplitude modulation in turbulent boundary layers, pipes, and channel flows. Physics of Fluids **21**(11), 111,703 (2009)
30. Moser, R.D., Kim, J., Mansour, N.N.: Direct numerical simulation of turbulent channel flow up to Re=590. Physics of Fluids **11**(4), 943–945 (1999)
31. Perry, A., Chong, M.: On the mechanism of wall turbulence. Journal of Fluid Mechanics **119**, 173–217 (1982)
32. Quadrio, M., Ricco, P.: Critical assessment of turbulent drag reduction through spanwise wall oscillations. Journal of Fluid Mechanics **521**, 251–271 (2004)
33. Quadrio, M., Ricco, P., Viotti, C.: Streamwise-travelling waves of spanwise wall velocity for turbulent drag reduction. Journal of Fluid Mechanics **627**, 161–178 (2009)
34. Ricco, P.: Modification of near-wall turbulence due to spanwise wall oscillations. Journal of Turbulence **5**(24) (2004)
35. Schlatter, P., rl, R.: Quantifying the interaction between large and small scales in wall-bounded turbulent flows: A note of caution. Physics of Fluids **22**(5), 051,704 (2010)
36. Skote, M.: Turbulent boundary layer flow subject to streamwise oscillation of spanwise wall-velocity. Physics of Fluids **23**, 081,703 (2011)
37. Skote, M.: Temporal and spatial transients in turbulent boundary layer flow over an oscillating wall. International Journal of Heat and Fluid Flow **38**, 1–12 (2012)
38. Skote, M.: Comparison between spatial and temporal wall oscillations in turbulent boundary layer flows. Journal of Fluid Mechanics **730**, 273–294 (2013)
39. Touber, E., Leschziner, M.A.: Near-wall streak modification by spanwise oscillatory wall motion and drag-reduction mechanisms. Journal of Fluid Mechanics **693**, 150–200 (2012)
40. Townsend, A.A.: The structure of turbulent shear flow. Cambridge university press (1980)
41. Viotti, C., Quadrio, M., Luchini, P.: Streamwise oscillation of spanwise velocity at the wall of a channel for turbulent drag reduction. Physics of fluids **21**(11), 115,109 (2009)
42. Wu, Z., Huang, N.: A study of the characteristics of white noise using the empirical mode decomposition method. In: Proceedings of the Royal Society of London A: Mathematical, Physical and Engineering Sciences, vol. 460, pp. 1597–1611. The Royal Society (2004)
43. Yudhistira, I., Skote, M.: Direct numerical simulation of a turbulent boundary layer over an oscillating wall. Journal of Turbulence **9**(12) (2011)
44. Zhang, C., Chernyshenko, S.I.: Quasisteady quasihomogeneous description of the scale interactions in near-wall turbulence. Physical Review Fluids **1**(1) (2016)